Physics Letters B 728 (2014) 136–140

Contents lists available at ScienceDirect

Physics Letters B

www.elsevier.com/locate/physletb

Towards the high spin–isospin frontier using isotopically-identified fission fragments

A. Navin [a,*], M. Rejmund [a], C. Schmitt [a], S. Bhattacharyya [b], G. Lhersonneau [a], P. Van Isacker [a], M. Caamaño [c], E. Clément [a], O. Delaune [a], F. Farget [a], G. de France [a], B. Jacquot [a]

[a] GANIL, CEA/DSM–CNRS/IN2P3, Bd Henri Becquerel, BP 55027, F-14076 Caen Cedex 5, France
[b] Variable Energy Cyclotron Centre, 1/AF Bidhan Nagar, Kolkata 700064, India
[c] USC, Universidad de Santiago de Compostela, E-15706 Santiago de Compostela, Spain

ARTICLE INFO

Article history:
Received 27 August 2013
Received in revised form 5 November 2013
Accepted 11 November 2013
Available online 22 November 2013
Editor: V. Metag

Keywords:
Isotopic identification
Fission fragments
Large isospin and high angular momentum
Neutron-rich Zr isotopes
Interacting boson model

ABSTRACT

Measurements of prompt γ rays in coincidence with isotopically-identified fission fragments, produced in collisions of ^{238}U on a ^{9}Be target, at an energy around the Coulomb barrier are reported. This technique provides simultaneous access to the spectroscopy of many nuclei, extending to very neutron-rich isotopes and fairly high angular momenta. The structural evolution of the neutron-rich zirconium isotopes is discussed in the light of the present measurements in ^{105,106}Zr and in the context of the interacting boson model with a global parameterization that includes triaxiality but no shape coexistence.

The fission process, though discovered more than 70 years ago, continues to be a fertile ground to study structural and dynamical aspects of quantum many-body systems [1]. It is also an important avenue for the production of nuclei far from stability. In fission reactions, several hundreds of nuclei around and far from the valley of stability are produced, with comparable excitation energies and fairly high angular momenta. These nuclei exhibit a variety of phenomena ranging from single-particle excitations near shell closures to collectivity resulting in vibrations or deformations, and can be used to probe the evolution of nuclear structure as a function of energy, angular momentum, and isospin (*i.e.*, neutron–proton asymmetry). Present and next-generation facilities, producing beams of nuclei far from stability, including those using the fission process, will provide unique opportunities in unraveling new features in both nuclear structure and reactions.

The use of de-exciting characteristic γ rays, first proposed more than 40 years back [2], is a powerful tool for the characterization of fission fragments. More recently, in extensive studies involving high-fold γ-ray coincidences, using the Gammasphere [3] and EUROBALL IV [4] arrays, in conjunction with either spontaneous-fission sources or in-beam measurements of heavy-ion induced fission reactions, a broad range of problems in nuclear structure [5,6] were investigated, including the response of nuclei at high angular momentum [7]. A majority of these measurements did not directly identify the nucleus of interest. This limited the study of very neutron-rich nuclei. In-beam γ-ray studies with radioactive-ion beams produced in fragmentation reactions, characterize nuclei near the limits of particle stability but generally at low angular momentum (with the exception of high spin isomers). The measurement of the response to extremes in both angular momentum and neutron–proton asymmetry, especially over long isotopic series, could lead to new discoveries and provide yet more stringent tests of our understanding of nuclear structure.

In this letter we report on in-beam studies of neutron-rich nuclei based on prompt γ-ray spectroscopy of isotopically-identified fission fragments which represents a step towards the study of nuclear properties as a function of *both* angular momentum and isospin. Of the large number of isotopes measured, the results for the very neutron-rich isotopes of zirconium ($Z = 40$) are presented. The Zr chain provides a long series of isotopes with varying properties: The neutron-deficient ^{80}Zr ($N = Z$) is found to be strongly deformed [8]. An addition of ten neutrons yields a doubly magic

* Corresponding author.
E-mail address: navin@ganil.fr (A. Navin).

0370-2693
http://dx.doi.org/10.1016/j.physletb.2013.11.024

spherical ^{90}Zr. Between N = 50 and N = 60 the Zr isotopes display a complex and rapidly changing behavior, presumably related to shape coexistence. It is still an open question whether this coexistent nuclear behavior persists beyond ^{100}Zr or there is return to a more normal, deformed state. Further towards the neutron dripline, exotic octupole (tetrahedral) shapes with a zero quadrupole moment are predicted around N = 70 [9], as well as 'giant' halos beyond N = 82 [10]. Additional interest in the neutron-rich Zr isotopes is raised by the recent observation of an unexpected long-lived isomer in ^{108}Zr [11,12], the nature of which is still unclear. The present work reports on the systematic investigation of the structure of ^{104,105,106}Zr to further understand the evolution of nuclear structure in neutron-rich Zr isotopes.

The measurements were performed at GANIL using a ^{238}U beam at 6.2 MeV/u (∼0.2 pnA), on a 10-micron thick ^{9}Be target. The advantage of the inverse kinematics is that the fission fragments are forward focused and have a large velocity, resulting in both an efficient detection and isotopic identification in the spectrometer. A single magnetic field setting of the large-acceptance spectrometer VAMOS++ [13,14] (momentum acceptance of around ±20%), placed at 20° with respect to the beam axis, was used to identify the fission fragments. The detection system (1×0.15 m^2) at the focal plane of the spectrometer was composed of (i) a Multi-Wire Parallel Plate Avalanche Counter (MWPPAC), (ii) two Drift Chambers (x, y), (iii) a segmented Ionization Chamber (ΔE), and (iv) 40 silicon detectors (E_r). The time of flight (TOF) was obtained from the two MWPPACs, one located after the target and the other at the focal plane (flight path ∼7.5 m). The measured parameters [(x, y), ΔE, E_r, TOF] along with the known magnetic field were used to determine, on an event-by-event basis, the mass number (A), charge state (q), atomic number (Z), and velocity vector ($\vec{v}$) for the detected fragment [13]. Improvements of the setup as compared to our earlier work [13–15] led to the isotopic identification of elements till Z = 63 with a mass resolution of $\Delta A/A \sim 0.4\%$. Fig. 1 shows the isotopic identification obtained in the present work. The prompt γ rays were measured in coincidence with the isotopically-identified fragments, using the EXOGAM array [16] consisting of 11 Compton-suppressed segmented clover HPGe detectors (15 cm from the target). The $\vec{v}$ of the fragment along with the angle of the segment of the relevant clover detector were used to obtain the γ-ray energy in the rest frame [17].

Fig. 2(a) shows the measured relative yields of the isotopically-identified fission fragments. The effect of the acceptance of VAMOS++ on the measured yields has been calculated based on the procedure discussed in Refs. [13,14]. The geometrical acceptance of VAMOS++ is around 13%–15%, for A ∼ 80–145 and rapidly drops to 7% for A ∼ 160 in the present case. The selection of VAMOS++ in the magnetic rigidity ($B\rho \sim Av/q$) further reduces the acceptance for the fragments with decreasing values of Z due to the dependence of q(Z, v). While the acceptance depends strongly on Z, being ∼2.0%, 5.0%, 7.5%, 6.0% for Z = 30, 40, 50 and 60 respectively, it has a weak dependence on A for a given Z. This variation is less than 0.5% within an isotopic chain. Hence the limit of the sensitivity of the measurement in reaching the most exotic nuclei is mainly constrained by the production mechanism itself. Also shown are the normalized results of PROFI calculations [18] corrected for the acceptance of VAMOS++. The PROFI code uses a semi-empirical description of the fission partition, including the excitation-energy-dependent influence of nuclear shell effects and pairing correlations. The model is used in the present work to calculate the isotopic yields of the fragments resulting from the decay of ^{247}Cm ($E^* \approx 45$ MeV) and ^{242}Pu ($E^* \approx 19$ MeV), arising from fusion- and α-transfer-induced fission, respectively. For an optimal reproduction of the experimental yields, the relative contributions of these processes are found to be around 80% and 20%, respectively, in agreement with earlier cross-section measurements [19]. The measured and calculated yields compare well in Fig. 2(a). The small observed differences in the tails suggest that the model predicts a slightly wider A and Z distribution. The measured yield of ^{106}Zr represents a small fraction (∼2.5×10^{-5}) of the total number of the isotopically-identified nuclei (∼400 different isotopes corresponding to various elements) detected in coincidence with prompt γ rays and highlights the large selectivity and sensitivity achieved. Besides its relevance for studying nuclear structure far from stability, the measurement of the complete mass and charge distribution populated by fission in coincidence with γ rays, reported here for the first time, are necessary to understand fundamental aspects of the fission mechanism [21].

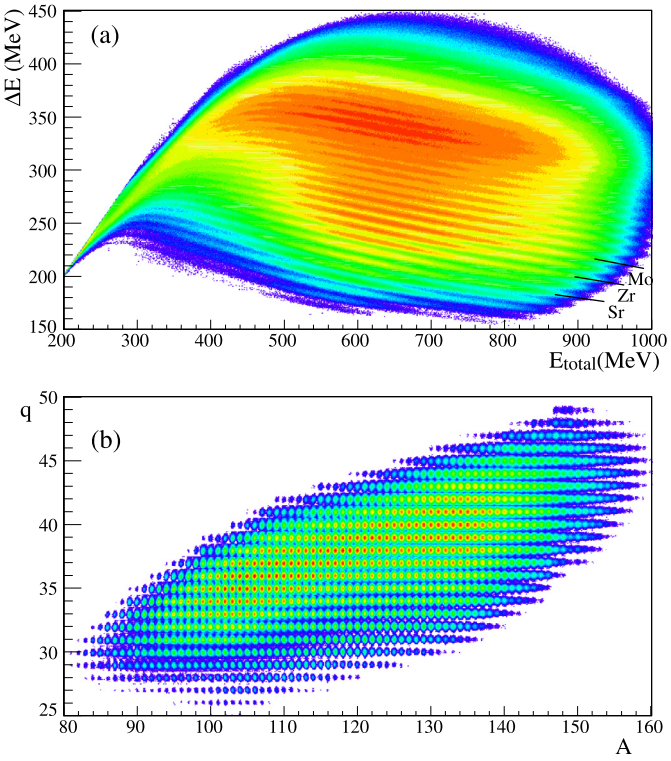

Fig. 1. (Color online.) (a) Two-dimensional spectrum of ΔE vs. E_{total} showing the Z identification of the various elements produced in the present work. The elements Sr, Zr and Mo are labeled. (b) Charge state (q) as a function of the mass number (A) of the measured fission fragments in the ^{238}U + ^{9}Be reaction at 6.2 MeV/u. The figure shows the large number of nuclei identified for a single setting of the spectrometer. A particular A and q in the plot can have contributions from more than one element (Z).

Fig. 2(b) displays the limits of detection, reached in studies of neutron-rich nuclei from Z = 38 to Z = 50, involving γ-ray spectroscopy. A more quantitative estimate of the measured γ-ray yields can be obtained from the following, γ-ray efficiency corrected, intensities for the 4^+ to 2^+ transitions for the even isotopes, ^{100}Sr: 713(80), ^{106}Zr: 278(70), ^{110}Mo: 1384(180), ^{114}Ru: 8527(470), ^{120}Pd: 6370(300) and ^{126}Cd: 777(300). The population of excited states through β decay depends on the J^π of the decaying parent nucleus, implying that high-spin states can be populated only in rare cases. Similarly, the detection of the γ decay of an isomer, *e.g.* at the focal plane of a separator, is also restrictive. The high-fold γ-coincidence method depends on both the ease of gating and the knowledge of the γ rays either from the relevant fragment or from its complementary fragments. The present method does not suffer from the above restrictions. Fig. 2(b) shows that the sensitivity of γ-ray spectroscopy reached in the present

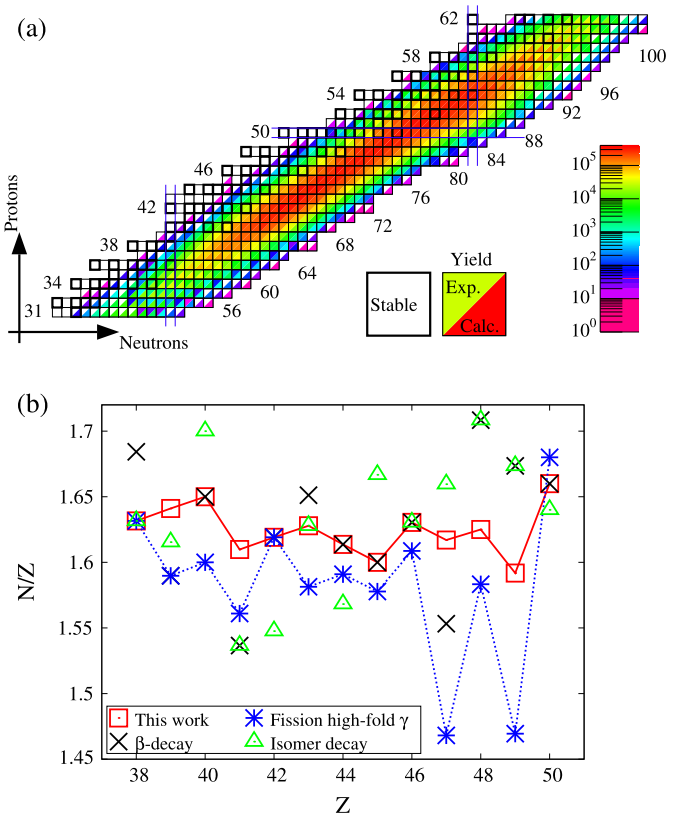

Fig. 2. (Color online.) (a) Segré chart for the relative yields of fission fragments, measured in VAMOS++ in coincidence with EXOGAM and the PROFI calculations [18] (see text). (b) N/Z ratio as function of Z for the most neutron-rich isotopes studied using γ-ray spectroscopy from the present work and those reported in the literature [20]. The lines are to guide the eye.

in-beam measurement of excited states in exotic nuclei is comparable to that obtained following *off*-beam β-decay measurements.

Fig. 3(a) shows the Doppler-corrected γ-ray energy as a function of the mass of the detected fragment for a specific isotopic chain. The evolution of nuclear structure as a function of neutron–proton asymmetry for a given isotopic (or isotonic) chain, can thus be directly visualized (from the change in the γ-ray energies as a function of mass) using these data from a single measurement. In addition to the Doppler-corrected γ-ray energies of the fragment detected in VAMOS++, the Doppler-corrected γ-ray spectrum of the undetected complementary fragment can also be obtained.

The Doppler-corrected γ-ray spectra of ^{104,105,106}Zr are shown in Fig. 3(b)–(d). Also shown in Fig. 3(b) is the γ-ray spectrum for the detected ^{104}Zr fragment but Doppler-corrected for the complementary fragment. Prior to the present work, no states in ^{105}Zr and, from β decay [11], only two states (2^+ and 4^+) in ^{106}Zr were known. Intensity and energy balance arguments, combined with the limited statistics of the coincidence data and a comparison with the systematics of lower-mass odd-N Zr isotopes [6,22], were used to suggest the level scheme of ^{105}Zr shown in Fig. 4. The placement of the 124(1), 161(3), 222(1), and 285(2) keV transitions (Fig. 3(c)) is confirmed from their definite coincidence relation, while indications for 319(1) and 374(1) keV transitions in the 222 keV gate were less conclusive. The 98(2) keV and 464(2) keV transitions could not be placed in the level scheme because of the lack of coincidence information. The spins of the states could not be measured directly. Hence tentative assignments (Fig. 4) were obtained based on the systematics for the observed band structure for lighter odd-N Zr isotopes. The ground-state configurations of ^{101}Zr and ^{103}Zr have been identified to be $5/2^-[532]$ [22] and

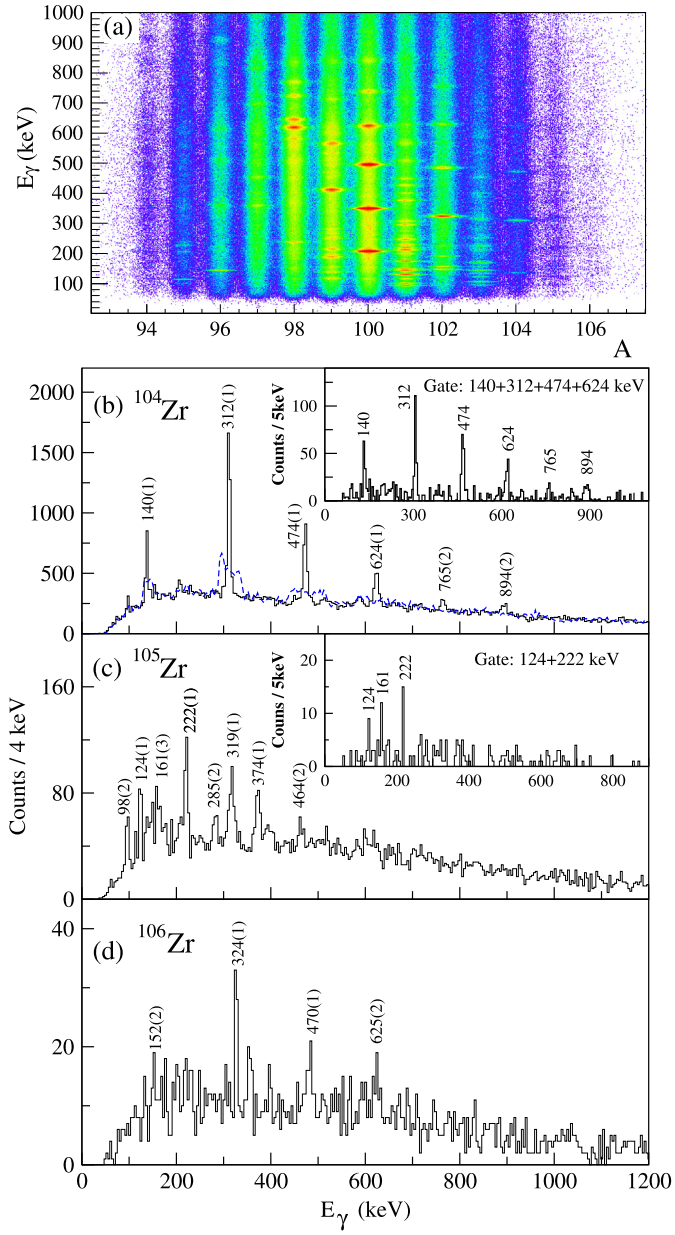

Fig. 3. (Color online.) (a) Doppler-corrected γ-ray energy as a function of the mass number of the Zr fragment identified in VAMOS++. (b), (c) & (d) The γ-ray spectra [projection of (a)] for the three most neutron-rich Zr isotopes measured in the present work, that is, for (b) ^{104}Zr, (c) ^{105}Zr and (d) ^{106}Zr. The inset of (b) & (c) shows the corresponding γ–γ coincidences. The dashed (blue) spectrum in (b) is the spectrum corrected for the corresponding complementary fragment.

$3/2^+[411]$ [23], respectively. The quasiparticle rotor model calculations [22] and the Projected Shell Model (PSM) calculations [24] predict the neutron $5/2^+[413]$ to be the lowest configuration for ^{105}Zr. The observed band is found to be consistent with such a $5/2^+$ assignment.

In ^{106}Zr, in addition to the known 152(2) and 324(1) keV γ rays [11], the two new transitions, 470(1) and 625(2) keV (Fig. 3(d)) are assigned to the decay of the higher-spin states of the ground-state band. The observed lower intensity of the 152(2) keV transition is attributed to an expected half-life of a few ns for the 2^+ state (similar to that reported in ^{104}Zr [25]) and in part due to the internal conversion ($\alpha = 0.242(7)$ [26]). The placement of the transition around 350 keV could not be made. The level scheme of ^{106}Zr, shown in Fig. 4, is constructed on the basis of ar-

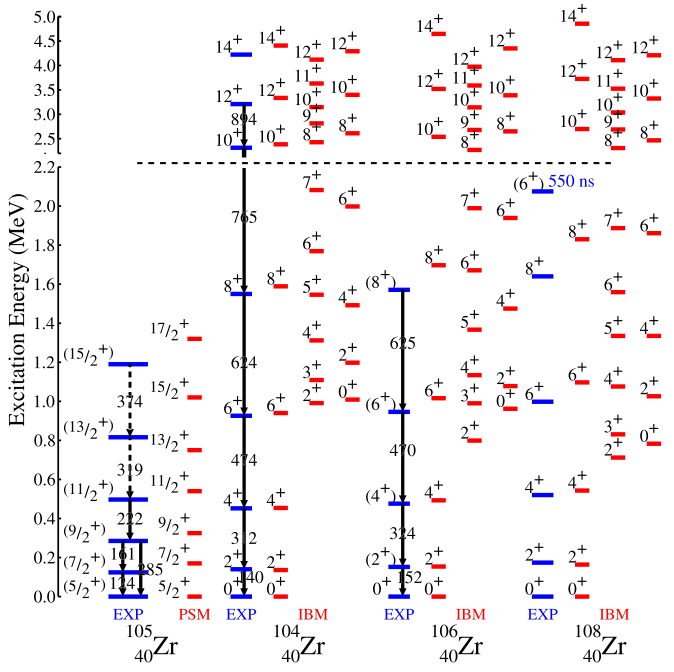

Fig. 4. (Color online.) Level schemes of the neutron-rich Zr isotopes proposed in this work. The γ rays shown in the figure are from the present work. The partial level scheme of ^{108}Zr is from Ref. [12]. Also shown are predictions of the Projected Shell Model [24] (^{105}Zr) and the global IBM calculation including triaxiality (^{104,106,108}Zr). The levels corresponding to different bands (see text) are suitably displaced.

guments related to intensity balance. The newly-observed higher-lying states cannot be populated in β decay, illustrating the general applicability of the present method to populate high-spin states in neutron-rich nuclei. Also shown in Fig. 4 is the tentative level scheme for ^{108}Zr, from the decay of the 550 ± 25 ns isomer [12]. The tentative assignment of the ^{108}Zr ground-state band (up to $J^\pi = 8^+$) [12] is strengthened by the newly-identified transitions in ^{106}Zr based on the smooth energy variation of the levels with neutron number seen in Fig. 5. The presence of a long-lived isomer in ^{108}Zr was unexpected, as no isomers have been reported in the neighboring ^{104,106}Zr and ^{110}Mo nuclei [11,12]. A spin and parity of 6^+ have been proposed for the isomer. This is based on calculations of two-quasiparticle states in a prolate deformed potential [27] that predicts single isomer ($K^\pi = 4^-$ at 1.41 MeV). From Ref. [12] it can be seen that the isomer decays to the 8^+ but that there are no transitions reported to the 4^+ and 6^+ levels of the ground-state band. This could indicate a higher spin for the isomer. It appears that the spin and the nature of the isomer in ^{108}Zr are still unclear for further work in the understanding of this unexpected isomer is necessary.

The structure of neutron-rich Zr isotopes has been discussed using a variety of approaches like PSM [24] and mean-field calculations [27,28]. The PSM correctly reproduces the measured energies of the yrast band in ^{104}Zr but increasingly deviates from the observed energies in the heavier Zr isotopes [24], indicating the need for further improvements in the model parameters. Mean-field calculations with the Gogny D1S interaction [28] systematically yield two coexisting minima for the Zr isotopes, of prolate and oblate deformation, separated by a shallow ridge in the triaxial plane. In this work the levels observed in the Zr isotopes are compared with the predictions of the interacting boson model (IBM), which is based on the assumption that nuclear collectivity can be expressed in terms of s and d bosons [29]. The simplest version of the model, IBM-1 which does not distinguish between neutron and proton bosons, is applied in a global fit to a region of the nuclear

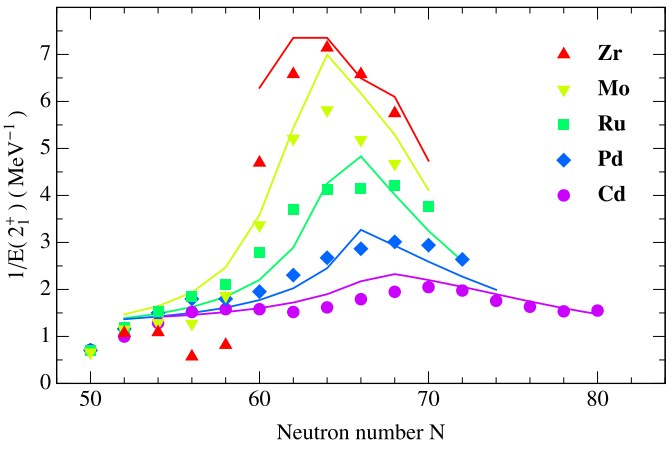

Fig. 5. (Color online.) The inverse of the excitation energy of 2_1^+ levels for a range of even-mass nuclei. The points are the observed energies [20] and the lines in the corresponding color represent the global IBM calculation.

chart in a parameterization similar to the one used in Ref. [30]. Calculations are limited to the even-mass Zr isotopes since a global parameterization for odd-mass nuclei with the interacting boson-fermion model [31] is currently not available.

The numbers of valence neutrons and protons, n and z, are counted from the closed shells $N = 50$ and $Z = 28$. The number of bosons is $N_b = N_\nu + N_\pi$ with $N_\nu = \min(n, (\Omega_\nu - 18 + z) - n)/2$ and $N_\pi = \min(z, \Omega_\pi - z)/2$, where Ω_ν and Ω_π are the neutron and proton shell sizes, respectively, $\Omega_\nu = 32$ and $\Omega_\pi = 22$. This defines an *effective* boson number that takes account of (sub-)shell effects for the neutrons which may depend on the number of protons. From studies with IBM-2 (which distinguishes between neutron and proton bosons) it is known that the Hamiltonian parameters are smooth functions of n and z [29], and in this study they vary linearly with n and z. The resulting Hamiltonian can be projected onto IBM-1, as long as no mixed-symmetry states are considered in the global fit. The global IBM-1 Hamiltonian used in this study therefore implicitly takes account of shell structure through the use of effective neutron and proton boson numbers of IBM-2.

A structural feature of many nuclei in this region is the presence of a $K^\pi = 2^+$ γ band at low energy, built on a vibrational mode that breaks axial symmetry. This indicates that (either rigid or soft) triaxiality plays an important role in the concerned nuclei. A cubic term is therefore added which introduces triaxial features in the IBM, in line with a recent microscopic derivation [32]. The adopted Hamiltonian is identical to the one of Ref. [33],

$$\hat{H} = \epsilon_d \hat{n}_d + \kappa\, \hat{Q} \cdot \hat{Q} + \kappa' \hat{L} \cdot \hat{L} + \lambda_d \hat{n}_d^2 + \upsilon_3 \left(d^\dagger \times d^\dagger \times d^\dagger\right)^{(3)} \cdot \left(\tilde{d} \times \tilde{d} \times \tilde{d}\right)^{(3)}, \quad (1)$$

where $\hat{n}_d$ is the d-boson number operator, $\hat{Q}_\mu = [d^\dagger \times \tilde{s} + s^\dagger \times \tilde{d}]^{(2)}_\mu + \chi [d^\dagger \times \tilde{d}]^{(2)}_\mu$ is the quadrupole operator and $\hat{L}$ is the angular momentum operator. The parameters in this Hamiltonian are varied linearly with numbers of valence neutrons and protons, in the spirit of the global fit of Ref. [30]. In all, 380 levels in 50 even-mass nuclei are considered, yielding a root-mean-square deviation of 127 keV. Fig. 5 illustrates a result of this global calculation, showing the evolution of the *inverse* of the excitation energy of the 2_1^+ level, $1/E_x(2_1^+)$, as a function of neutron and proton numbers. This is a sensitive indicator of shell and sub-shell structure, the effects of which can be accounted for with an effective boson number. The pathological behavior of the $^{90-98}$Zr nuclei, associated with the combined sub-shells at $N = 50, 56$ and $Z = 40$ is

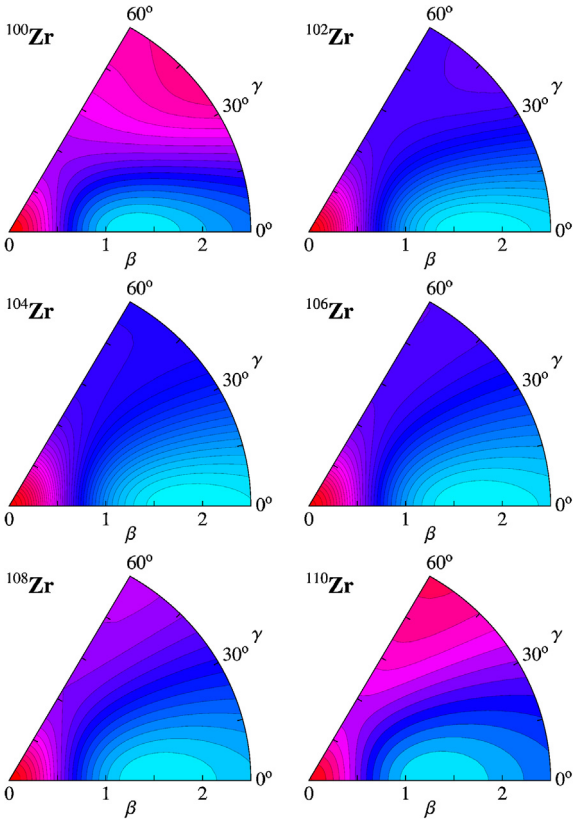

Fig. 6. (Color online.) Total energy surfaces in the (β, γ) plane, as derived from the IBM Hamiltonian, for $^{100-110}$Zr isotopes included in the fit. Minima are in blue and maxima in red. The energy difference between the successive contour lines is 100 keV.

a special feature of this isotope series (seen from the rapidly varying $1/E_x(2_1^+)$ values). Sudden shell effects cannot be accounted for in a global description with a collective model, and therefore the $^{90-98}$Zr nuclei have been omitted from the fit. In marked contrast with the mean-field results of Ref. [28], no shape coexistence mechanism is invoked in the global IBM calculation to explain the low-energy structure of the nuclei included in the fit and all 0_2^+ levels are explained as collective excitations, and not as coexisting states with a different shape. This observation is consistent with the (β, γ) total energy surfaces, derived from the IBM Hamiltonian for all nuclei, which always display a single minimum and no shape coexistence. As an example, the total energy surfaces for the Zr isotopes are shown in Fig. 6. Within the current parameterization (accounting for triaxiality), the 2_2^+ level is calculated at 799 keV in ^{106}Zr and rapidly drops in energy with increasing neutron number. The present calculation suggests that the 607 keV γ-ray previously assigned to the $2_2^+ \rightarrow 0_1^+$ in ^{106}Zr [11], is more likely to be associated with the $2_2^+ \rightarrow 2_1^+$.

In summary, in-beam γ-ray spectroscopy of isotopically-identified neutron-rich fission fragments, complementary to those obtained from β decay at isotope separators or through multiple coincidences with γ-ray detector arrays, are reported. In particular, results on the prompt γ spectroscopy of the neutron-rich ^{105,106}Zr isotopes are presented, and interpreted in an improved global IBM calculation that includes triaxial deformation. The present work shows that their structure changes rather smoothly as a function of N consistent with nuclei in this region and there are no surprises unlike the presence of an unexpected isomer in ^{108}Zr as reported by Refs. [11,12]. The obtained fission-fragment mass distribution extended to fragments with large N/Z at relatively large angular momentum. Thus the present method when coupled with new-generation γ-ray tracking detector AGATA [34] to EXOGAM and VAMOS++, exploiting both stable and next-generation ISOL beams, will open avenues for understanding nuclei under extreme conditions of neutron–proton asymmetry *and* angular momentum and also enable detailed investigation of the fission mechanism.

Acknowledgements

We would like to thank J. Goupil, G. Fremont, L. Ménager, J. Ropert, C. Spitaels, and the GANIL accelerator staff for their technical contributions. One of us (S.B.) acknowledges partial financial support through the LIA France–India agreement.

References

[1] K.-H. Schmidt, Lecture notes Ecole Joliot Curie, http://ejc2011.sciencesconf.org/resource/page?id=28, 2011.
[2] H.R. Bowman, S.G. Thompson, J.O. Rasmussen, Phys. Rev. Lett. 12 (1964) 195; E. Cheifetz, R.C. Jared, S.G. Thompson, J.B. Wilhelmy, Phys. Rev. Lett. 25 (1970) 38.
[3] http://www.phy.anl.gov/gammasphere.
[4] http://euroball.lnl.infn.it/.
[5] J.H. Hamilton, et al., Prog. Part. Nucl. Phys. 35 (1995) 635; I. Ahmad, W. Phillips, Rep. Prog. Phys. 58 (1995) 1415.
[6] H. Hua, et al., Phys. Rev. 69 (2004) 014317.
[7] E.S. Paul, et al., Phys. Rev. Lett. 98 (2007) 012501; M. Riley, et al., Phys. Scr. T 125 (2006) 123.
[8] C.J. Lister, et al., Phys. Rev. Lett. 59 (1987) 1270.
[9] N. Schunck, J. Dudek, A. Góźdź, P.H. Regan, Phys. Rev. C 69 (2004) 061305(R).
[10] J. Meng, P. Ring, Phys. Rev. Lett. 80 (1998) 460.
[11] T. Sumikama, et al., Phys. Rev. Lett. 106 (2011) 202501.
[12] D. Kameda, et al., Phys. Rev. C 86 (2012) 054319.
[13] M. Rejmund, et al., Nucl. Instrum. Methods Phys. Res., Sect. A 646 (2011) 184.
[14] S. Pullanhiotan, et al., Nucl. Instrum. Methods Phys. Res., Sect. A 593 (2008) 343.
[15] A. Shrivastava, et al., Phys. Rev. C 80 (2009) 051305.
[16] J. Simpson, et al., Acta Phys. Hung., New Ser., Heavy Ion Phys. 11 (2000) 159.
[17] S. Bhattacharyya, et al., Phys. Rev. Lett. 101 (2008) 032501.
[18] J. Benlliure, A. Grewe, M. de Jong, K.-H. Schmidt, S. Zhdanov, Nucl. Phys. A 628 (1998) 458.
[19] R. Raabe, et al., Phys. Rev. C 74 (2006) 044606.
[20] ENSDF database, http://www.nndc.bnl.gov/endsf.
[21] F. Farget, et al., J. Phys. Conf. Ser. 420 (2013) 012119.
[22] W. Urban, et al., Phys. Rev. C 79 (2009) 067301.
[23] M.A.C. Hotchkis, et al., Phys. Rev. Lett. 64 (1990) 3123.
[24] Y.X. Liu, et al., Nucl. Phys. A 858 (2011) 11.
[25] J. Hwang, et al., Phys. Rev. C 73 (2006) 044316.
[26] T. Kibédi, et al., Nucl. Instrum. Methods Phys. Res., Sect. A 589 (2008) 202.
[27] Y. Shi, P.M. Walker, F.R. Xu, Phys. Rev. C 85 (2012) 027307.
[28] J.-P. Delaroche, et al., Phys. Rev. C 81 (2010) 014303.
[29] F. Iachello, A. Arima, The Interacting Boson Model, Cambridge University Press, Cambridge, 1987.
[30] M. Böyükata, P. Van Isacker, İ. Uluer, J. Phys. G, Nucl. Part. Phys. 37 (2010) 105102.
[31] F. Iachello, P. Van Isacker, The Interacting Boson-Fermion Model, Cambridge University Press, Cambridge, 1991.
[32] K. Nomura, N. Shimizu, D. Vretenar, T. Nikšić, T. Otsuka, Phys. Rev. Lett. 108 (2012) 132501.
[33] B. Sorgunlu, P. Van Isacker, Nucl. Phys. A 808 (2008) 27.
[34] S. Akkoyun, et al., Nucl. Instrum. Methods Phys. Res., Sect. A 668 (2012) 26.